Analysis of Antichiral Thermomechanical Metamaterials with Continuous Negative Thermal Expansion Properties

Debajyoti Saha[1], Paul Glanville[2], and Eduard G. Karpov[1,*]
[1]*Department Civil & Materials Engineering, University of Illinois, Chicago, IL 60607, U.S.A.*
[2]*Gas Technology Institute, Des Plaines, IL 60018, U.S.A.*
**Corresponding author, email: ekarpov@uic.edu*

Abstract: Negative thermal expansion phenomenon is interesting and appealing for various scientific and engineering applications, while rarely occurring in natural materials. Here, using a universal antichiral metamaterial model with bimetal beams or strips, a generic theory has been developed to predict magnitude of the negative thermal expansion effect from the model parameters. Thermal expansivity of the metamaterial is written as an explicit function of temperature and only three design parameters: relative node size, chirality angle, and a bimetal constant. Experimental measurements follow theoretical predictions well, where a thermal expansivity in the range of negative 0.0006-0.0041$^{o}C^{-1}$ has been seen.

1. Introduction & Material System Definition

Metamaterials is a term that defines modern engineered materials with extreme properties and functionalities that are not available in natural materials. Veselago in 1967 [1] proved theoretically that materials with both negative permeability and negative permittivity could demonstrate a range of unprecedented properties varying from light source attraction to flat lens focusing. Later Pendry and Smith [2-4] expanded these concepts to advanced resolution imaging and wave guiding technology [5-9]. The term metamaterials, though, was only first used by Walser in 2001 [10]. The prefix *meta* stands for Greek *beyond* or *after*, implying availability of additional dimensions in the property space of metamaterials when compared to the usual materials. A major advancement seen in more recent literature is a realization that the reverse or expanded properties can be realized in an "effective" manner, from material responses only to certain excitation frequencies. Thus, a key concept of frequency-dependent material property, varying from positive to negative or even complex values, has emerged and flourished. This contrasted with the original idea of a negative material property viewed in an objective manner, as a basic frequency-independent material constant [1] that is much more difficult to achieve in practice. In particular, the concept of negative refractive index has also been seen in wave mechanics and phononics, where it is associated with negative effective bulk modulus and negative effective mass density, observed at certain frequency ranges of an incident acoustical signal. Newly realized phenomena of shielding, bending and focusing of sound waves propagating through materials with those reverse effective properties could serve for many interesting practical applications [11-14].

The notion of a *mechanical* metamaterial is the most recent and emerging in the field. The main objective of research in the area of mechanical metamaterials is to demonstrate materials with exotic mechanical properties, such as Poisson's ratio, Young's modulus, bulk and shear moduli. The successes in the field of optics and acoustics, enabled by the material's internal structure engineering, have guided the theory and application of mechanical metamaterials. A common approach shared by most authors in the field is to view the unusual mechanical properties as a result of a smart internal structure of the metamaterial at a unit cell level [15-23]. A proper engineering design then may lead to some extreme properties which are not available in the base materials used to fabricate those structures. For example, Kolpakov [17] and Lakes [18-19] described latticeworks and polyform foam structures with negative Poisson's ratios [17] that would expand laterally when a longitudinal tensile force is applied. This type of nonconvex microstructures can be interesting for aerospace and marine application because their good absorption and light weight properties [20-21]. Many interesting properties and behaviors are realized from *bistable* unit cell designs in periodic metamaterials, including highly efficient energy damping and trapping [22-23], negative stiffness [24], as well as negative incremental compressibility [25-28] and extensibility [29-30]. Other studies of materials with engineered internal structure showed opportunities for a Saint-Venant's edge effect reversal [31], strain energy control and redirection by demand [32-34], loss of reciprocity of materials deformation [35], and for a negative thermal expansion phenomenon [36-40]. Harnessing these advanced behaviors could enable many exciting solutions in architecture, energy systems, manufacturing industry, transportation, and other areas.

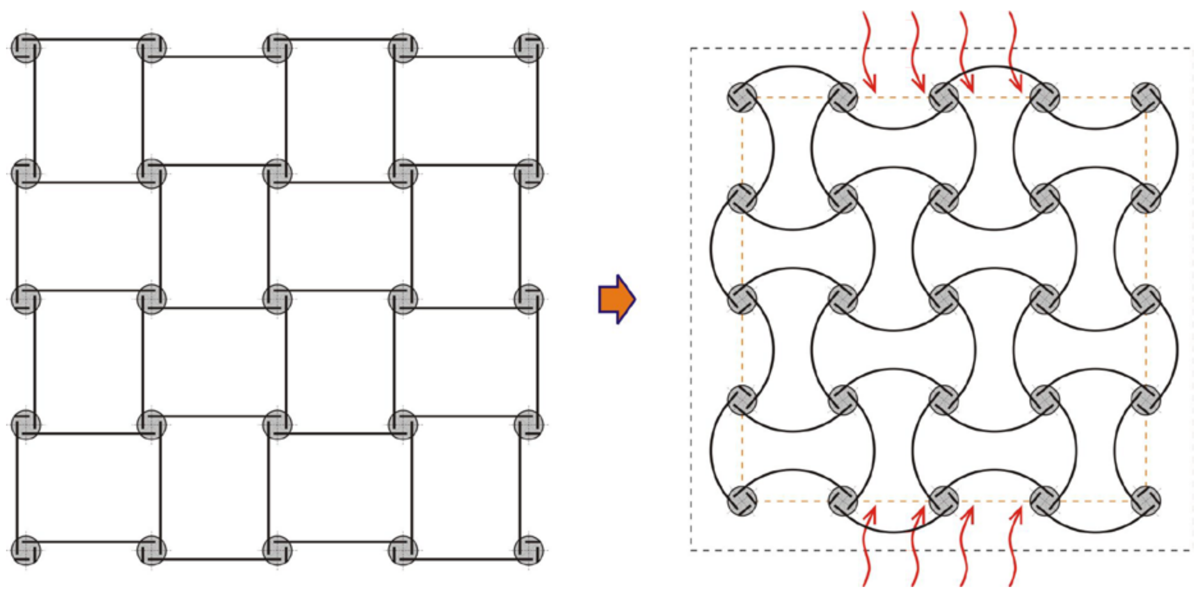

Figure 1.1: Antichiral metamaterial architecture, enabling negative (effective) thermal expansion. Continuous elastic thermal buckling of the bimetal strips, shown as solid lines, leads to an overall contraction of the material sample with temperature.

The main objective of this work is to provide a solid theoretical basis, backed up by experimental measurements, for a class of antichiral thermomechanical metamaterials with negative thermal expansion properties and continuous (non-snapping) responses to thermal loads. A recent review of the chiral metamaterial architectures is provided in [40]. One example from the literature, e.g. [38,40-41], is shown in Figure 1.1. Here, the bimetal strip materials have a mismatch of their thermal expansion coefficients, leading to a continuous thermal bending of the strips and overall size reduction of the material sample with temperature. A similar geometry was also discussed in the context of continuous negative thermal expansion, which can be realized from a hydrostatic mechanical pressure applied to both sides of the bimetal strips that have a mismatch of elastic properties of the two materials [41]. In this paper, though, we focus on *thermal* responses of the Figure 1.1 geometry. We also extend it to a *generic antichiral geometry* with arbitrary node shape/size, chirality angle and bimetal constant, and study dependence of the negative thermal expansion characteristics on these design parameters.

Our generic metamaterial model is comprised of multiple bimetal *strips* of equal length and repeating solid *nodes* serving to connect the strips together. In practice, circular nodes with openings for strip insertion and fixture can be used for an arbitrary ***chirality angle***, θ_0, see Figure 1.2 (left). Alternatively, the strips can be attached to side surfaces of polygonal of circular nodes for a specific value of the chirality angle (45°, 60° or 90°), see Figure 1.2. The chirality angle is therefore a variable design parameter of this material system. It is generally defined as a minimal nonzero angle between a vertical symmetry axis of the material and a line passing through the node center and an endpoint of the free-standing part of a strip. Note that in all cases, portions of the bimetal strip in contact with nodes are assumed to be rigidly attached to the nodes in a nonslip manner. The remaining portion of the strips is *free-standing*, able of reversible mechanical buckling (bending) with heating or cooling, see drawings in Figures 1.2 and 1.3.

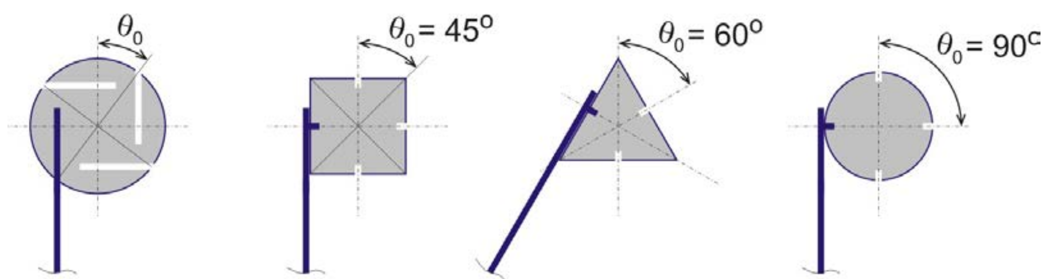

Figure 1.2: Definition of the chirality angle θ_0, as a variable system parameter, and special cases of this angle for metamaterials with solid nodes of square, triangular and circular shapes.

Figure 1.3 drawing explains that three geometrical parameters, the chirality angle θ_0, the node radius R (distance from node center to an endpoint of the free-standing part of a bimetal strip), and length L of the free-standing parts of the bimetal strip fully defines the material's internal architecture. We also introduce a single *state parameter*, which is the ***angle of rotation*** of the nodes θ, see Figure 1.3, to describe a state of deformation of the material due to heating. This state of deformation is defined by thermal bending of the bimetal strips upon uniform temperature change of the material, ΔT, with respect to an initial temperature at which all the strips are straight. Curvature of a thermally buckled strip is known to be uniform, so that the entire free standing strip takes a circular arch shape [42]. Therefore, from Figure 1.3,

$$\theta = \frac{L}{2\rho} \tag{1}$$

where ρ is a uniform radius of curvature of the bimetal strips. It is interesting to note (e.g., from [42]) that dependence of the curvature on a temperature change is linear. Therefore, we suggest to introduce a system parameter, a, unique for a given bimetal strip, such that $a\Delta T = 1/\rho$, and to write a linear constitutive relationship between the angle of deformation and temperature,

$$\theta = \frac{L}{2\rho} = \frac{aL\Delta T}{2} \qquad (2)$$

The coefficient *a* can be interpreted as the bimetal strip's *specific thermal bending coefficient* (per unit length), which gives an amount of uniform bending deformation (in radians) per one-degree temperature change. The dimensionality of *a* is $[L^{-1}T^{-1}]$, and its value depends on the cross-section geometry of the bimetal strip, elastic and thermal expansion coefficients of the two metals and their joining fabrication method. Because of these multiple factors, the thermal bending coefficient, *a*, in (2) should generally be found experimentally, using its physical meaning. More details are given Section 3.

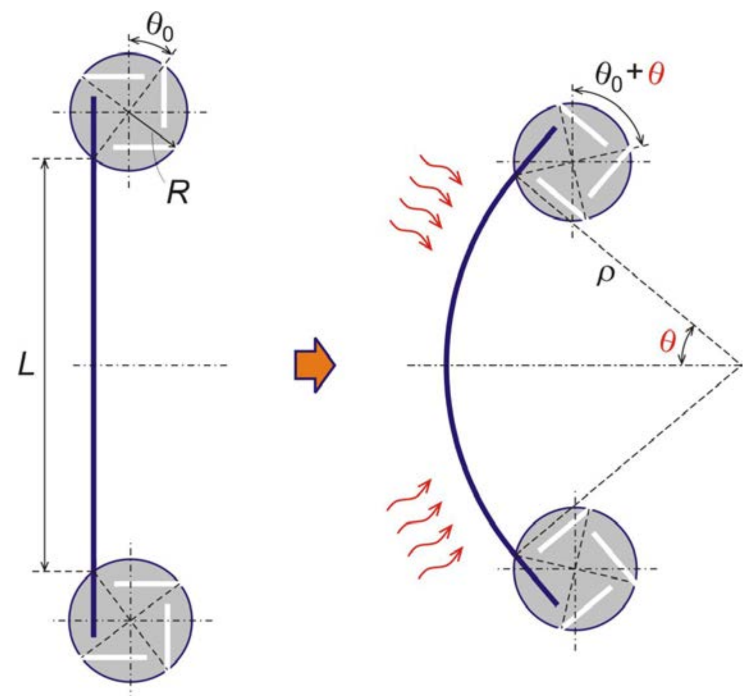

Figure 1.3: Three geometrical parameters of the metamaterial's internal architecture (θ_0, R and L), and the node rotation angle (θ), as a single parameter to describe a thermally induced state of deformation. Here, $\rho = L/\theta$ is a radius of curvature of the thermally deformed strip.

2. Theoretical Analysis

In this section, we discuss a quantitative analysis method, definitions of thermal expansion characteristics of the antichiral metamaterials, and predictions of their values from key structural parameters, accompanied by practical design recommendations.

Some basic quantities that will be used in the analysis are the following. According to Figure 1.3, the *original distance* between centers of two nodes, when the strips are straight, at $\Delta T = 0$,

$$l_0 = L + 2R\cos\theta_0 \tag{3}$$

Then, a *deformed distance* between centers of two nodes, after application of heat to the system,

$$l_T = \frac{L_T}{\theta}\sin\theta + 2R_T\cos(\theta + \theta_0) \tag{4}$$

Here, L_T is a changed length of the strip after temperature is applied, R_T is a changed radius of the nodes due to the temperature, θ is a node rotation angle, and θ_0 is a constant chirality angle as in Figure 1.2.

The values L_T and R_T can be written in a standard form using the *usual* coefficients of linear thermal expansion of the strip material, α_s (cumulative), and of the node material, α_n,

$$L_T = L(1 + \alpha_s\Delta T) \tag{5}$$

$$R_T = R(1 + \alpha_n\Delta T) \tag{6}$$

These provide a distance between two nodes in a thermally deformed configuration in the form,

$$l_T = (1 + \alpha_s\Delta T)\frac{L\sin\theta}{\theta} + 2R(1 + \alpha_n\Delta T)\cos(\theta + \theta_0), \qquad \theta = \frac{aL\Delta T}{2} \tag{7}$$

2.1. Thermal Strain Function

The quantities l_0 and l_T given by equations (3) and (7) represent an original length and a deformed length of a repeating unit cell of the metamaterial. Therefore, we can write the thermal strain as

$$\varepsilon_T = \frac{l_T - l_0}{l_0} = \frac{2\theta R(1+\alpha_n\Delta T)\cos(\theta+\theta_0) + L(1+\alpha_s\Delta T)\sin\theta}{\theta(L + 2R\cos\theta_0)} - 1 \tag{8}$$

The values of α_n and α_s are from 10^{-6} to 10^{-5} °C^{-1} in metal alloys, and we may often encounter a situation when $\alpha_{s,n} \ll aL$ for the metamaterials discussed here. If $\alpha_{s,n}/aL < 10^{-3}$, the usual thermal expansion will have a practically negligible effect on the thermal strain (8) behavior. In this case, internal *structural* parameters of the metamaterial will *dominate* its effective thermal expansion properties. Looking at equation (8) we realize that the thermal strain depends on a ratio R/L only, rather than separately on R and L. Moreover, the angle θ depends only on a product aL, and not separately on a and L. Thus, the number of ***independent structural parameters*** is only three (θ_0, r and aL), see Table 1.

Table 1: Independent structural parameters of the antichiral metamaterial

Chirality angle (rad)	Node size ratio	Thermal bending coefficient (rad/°C)
$\boldsymbol{\theta_0}$	$\boldsymbol{r = \frac{R}{L}}$	$\boldsymbol{A = aL}$

A final form of the ***thermal strain***, as a function of only independent structural parameters and temperature, reads

$$\varepsilon_T = \frac{2\theta r(1+\alpha_n\Delta T)\cos(\theta+\theta_0)+(1+\alpha_s\Delta T)\sin\theta}{\theta(1+2r\cos\theta_0)} - 1, \qquad \theta = \frac{aL\Delta T}{2} = \frac{A\Delta T}{2} \tag{9}$$

In Figure 2.1, we show behavior of this function at some finite ratios r, and fixed a and R used in the experiments that will be described later in Section 3. Figure 2.1 also shows a *relative surface area reduction* of the metamaterial, $A_T/A_0 = (\varepsilon_T + 1)^2$, where $A_0 = l_0^2$ and $A_T = l_T^2$ are initial and reduced areas, respectively. This property could be interesting for autonomous safety systems applications of the present metamaterials, for example, serving to reduce throughput of pipes and vents with temperature.

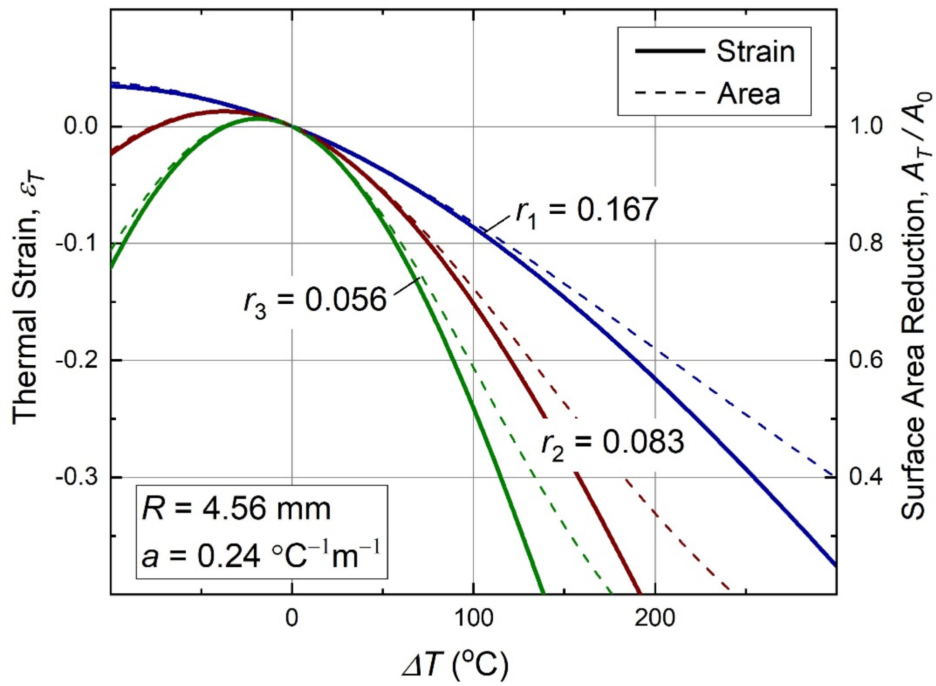

Figure 2.1: Behavior of the thermal strain (9) with temperature in the antichiral thermomechanical metamaterials of Figure 1.1 type. The thermal strain is always negative at positive ΔT, and its overall behavior is nonlinear. Relative surface area reduction of a material sample, $A_T/A_0 = (\varepsilon_T + 1)^2$, is shown with dash lines. For these and all further data plots, $\alpha_{s,n} \approx 10^{-3}aR/r$, when the curve shapes are dominated by the metamaterial's geometry, and the effect of natural thermal expansion is negligible.

2.2. Thermal Expansivity Function

The thermal strain (9) is a nonlinear function of temperature, even at $\Delta T \approx 0$. Therefore, we introduce a ***thermal expansivity*** function, $\alpha_T = \alpha_T(\Delta T)$, rather than a constant coefficient, as a derivative,

$$\alpha_T = \frac{d\varepsilon_T}{d(\Delta T)} = \frac{2(1+\Delta T\alpha_s)\theta\cos\theta + 4r\Delta T\alpha_n\theta\cos(\theta+\theta_0) - 2\sin\theta - 4r(1+\Delta T\alpha_n)\theta^2\sin(\theta+\theta_0)}{2\Delta T\theta(1+2r\cos\theta_0)} \tag{10}$$

For the three different node size ratios, behavior of this function with temperature is shown in Figure 2.2. As can be seen, it can be non-monotonous, because of the sine and cosine functions involvement in the temperature dependence. Also, *negative* thermal expansivity is better pronounced at higher nodal size ratios, r, which occurs in the denominator of the equation (10).

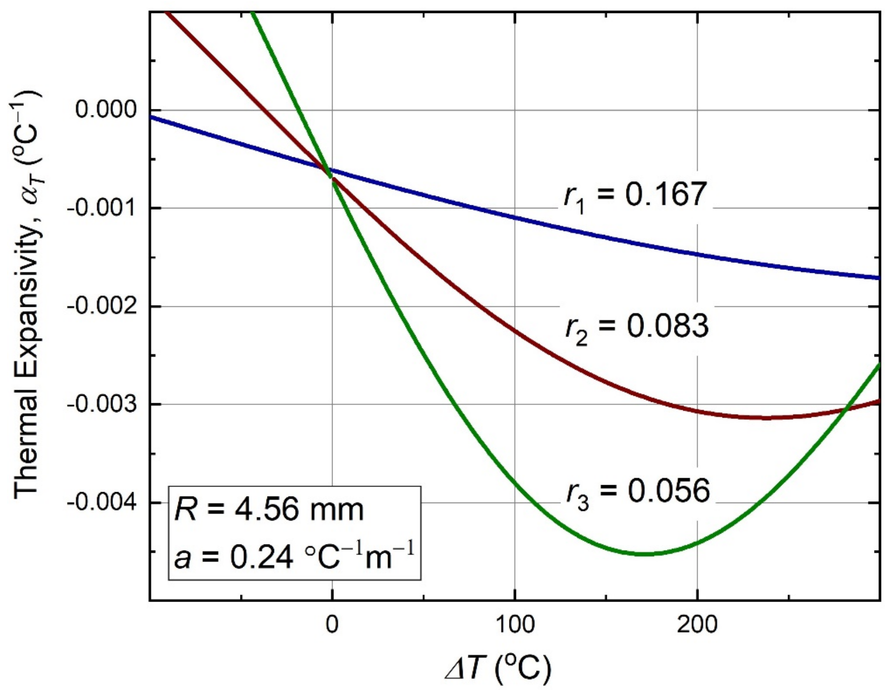

Figure 2.2: Thermal expansivity (10) of the antichiral metamaterial as function of temperature.

2.3 Thermal Hyperexpansivity

A derivative of the thermal expansivity function (10) with respect to temperature can be referred to as ***thermal hyperexpansivity,***

$$\alpha_T' = \frac{d\alpha_T}{d(\Delta T)} = -\frac{2\theta\cos\theta + 2r(1+\Delta T\alpha_n)\theta^3\cos(\theta+\theta_0) - 2\sin\theta + \theta^2\sin\theta + \Delta T\theta^2(\alpha_s\sin\theta + 4r\alpha_n\sin(\theta+\theta_0))}{(\Delta T)^2\theta(1+2r\cos\theta_0)} \quad (11)$$

Plot of this function versus temperature, for the same three nodal size ratios, as in the previous plots of ε_T and α_T, are shown in Figure 2.3.

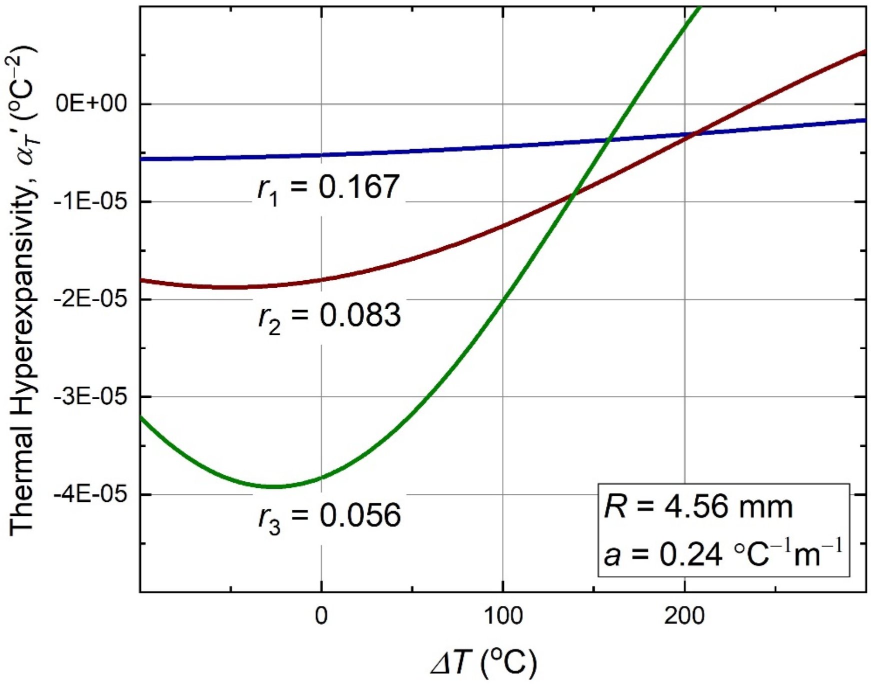

Figure 2.3: Thermal hyperexpansivity (11) of the antichiral metamaterial as function of temperature.

2.4. Initial Thermal Expansivity and Hyperexpansivity

Thermal expansivity of the antichiral metamaterial has a negative slope versus temperature at all combinations of the system parameters, see Figure 2.2 for an illustration, and a temperature increase further enhances magnitude of the negative thermal expansion effect. Therefore, for many practical purposes, it is interesting to study dependence of the initial (at $\Delta T \approx 0$) values of the functions α_T and α_T' on the system parameters. A combination of parameters at which these functions attain maximal possible (by modulus) values could be viewed as recommendations for the practical material design.

If we employ a single parameter for the usual thermal expansion, $\alpha_s = \alpha_n$, recall that $\theta = aL\Delta T/2$, and apply a power series decomposition of the thermal strain (9) at $\Delta T = 0$ up to a quadratic term,

$$\varepsilon_T \approx \alpha_0 \Delta T + \alpha_0' \frac{(\Delta T)^2}{2} = \frac{\alpha_s(1+2r\cos\theta_0) - aLr\sin\theta_0}{1+2r\cos\theta_0}\Delta T - \frac{(24\alpha_s r\sin\theta_0 + aL + 6aLr\cos\theta_0)aL}{12+24r\cos\theta_0}\frac{(\Delta T)^2}{2} \quad (12)$$

we may interpret the coefficient α_0 at the linear term as an ***initial thermal expansivity*** (at $\Delta T \approx 0$). This characteristic can be written in an interesting shorter form, a sum of the natural thermal expansion (α_s), and a term depending only on the architectural design parameters (θ_0, r and aL):

$$\alpha_0 = \alpha_s - \frac{raL\sin\theta_0}{1+2r\cos\theta_0} \quad (13)$$

Obviously, the first term can be ignored, if $\alpha_s \ll aL$. A practical range of the chirality angle is from 0° to 90°, because values higher than 90° would require practically impossible connections to accommodate overlapping bimetal strips. We assumed some fixed values of θ_0 and aL, as were later used in the experiments, and plotted α_0 onto the contour maps of Figure 2.4. They reveal a monotonous dependence of α_0 on all the independent structural parameters of the metamaterial, so that a greater negative thermal expansion effect at $\Delta T \approx 0$ should generally be expected at larger values of θ_0, r and aL.

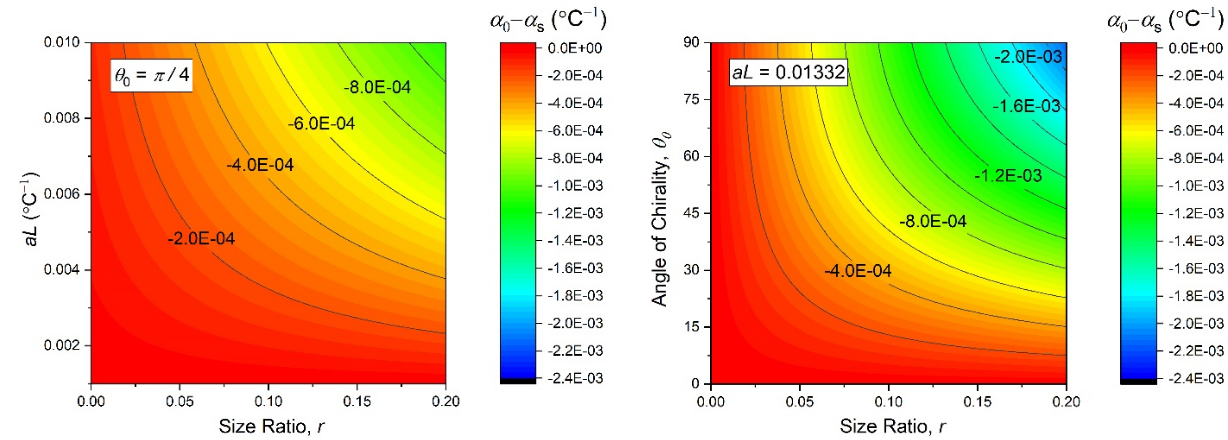

Fig.2.4: Contour plots of the initial thermal expansivity (13), as function of the independent design parameters (θ_0, r and aL).

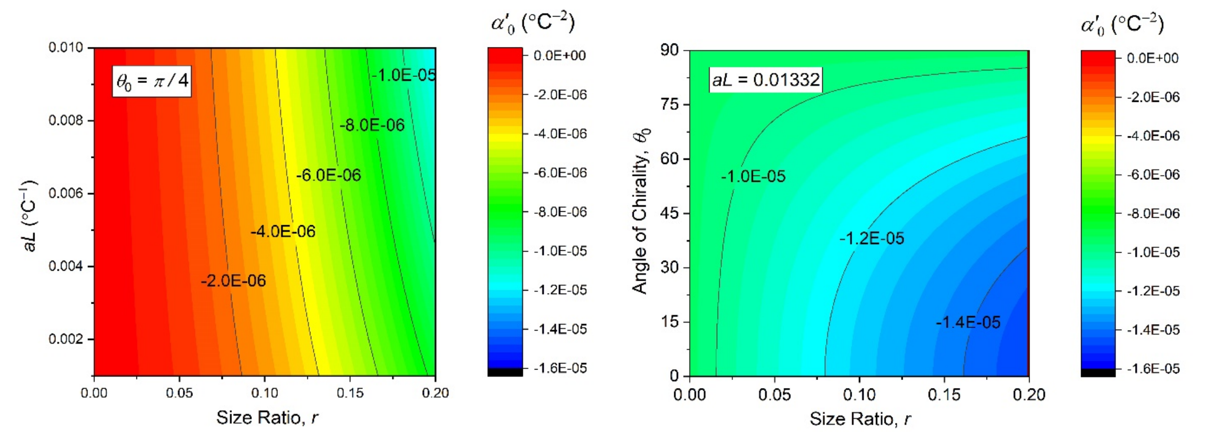

Fig.2.5: Contour plots of the initial thermal hyperexpansivity (14) as function of the independent design parameters (θ_0, r and aL).

From the power series expansion of the thermal strain (12), we may also define an ***initial hyperexpansivity*** of the antichiral metamaterial (at $\Delta T \approx 0$ and $\alpha_s \ll aL$),

$$\alpha'_0 = -\frac{aL(aL + 6aLr\cos\theta_0)}{12 + 24r\cos\theta_0} \tag{14}$$

which is also monotonous with θ_0, r and aL, although a greater hyperexpansivity should be expected at smaller chirality angles, see Figure 2.5.

2.5. Maximal Rotation Angle & Temperature

Continuous thermal deformation in the antichiral metamaterials discussed here might be restrained in practice, because of a possible limiting configuration depicted in Figure 2.6. Here, two opposite bimetal strips in a unit cell encounter each other due to an excessive thermal deformation. This situation is unique for a particular metamaterial design $\{\theta_0, r, aL\}$, and it is described by some nodal rotation angle, θ_{m}, a *maximal angle* of applicability of the theory discussed here.

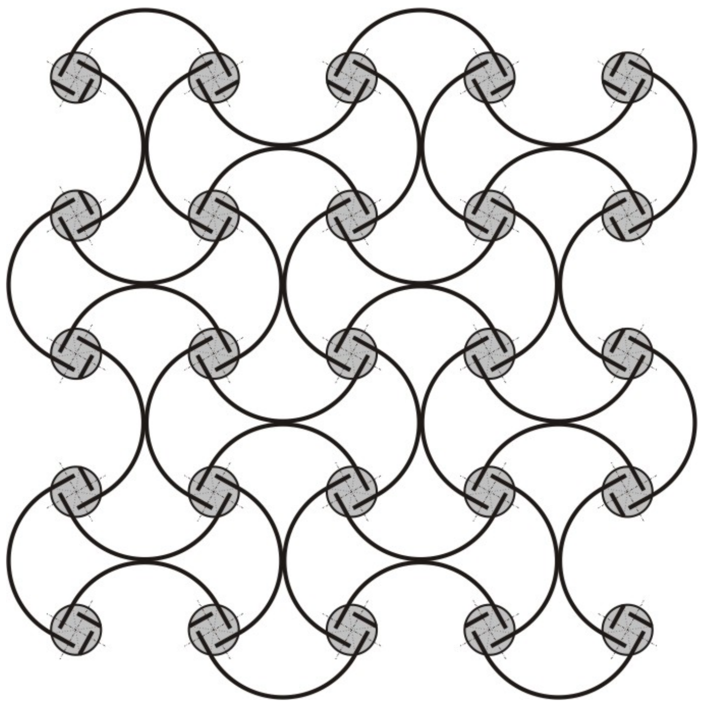

Fig.2.6: Occurrence of a maximal angle of nodal rotation, θ_{m}, in the antichiral thermomechanical metamaterial of Figure 1.1 type.

This angle can be determined from a condition that the deformed distance (7) between two nodes is equal to a double distance between the middle arch point of a bimetal strip, attached to these nodes, and the base line passing through the centers of these nodes. The usual thermal expansion has a negligible effect on the maximal angle value, when $\alpha_s, \alpha_n \ll aL$. These to lead a ***maximal angle condition*** in the form,

$$\frac{\sin\theta_m}{\theta_m} + 2r\cos(\theta_m + \theta_0) = \frac{1-\cos\theta_m}{\theta_m} + 2r\sin(\theta_m + \theta_0) \qquad (15)$$

The corresponding maximal operational temperature of the metamaterial is simply

$$\Delta T_m = \frac{2\theta_m}{aL} \qquad (16)$$

The transcendental equation (15) is not solvable in a closed form for θ_m. We solved is numerically and mapped the solution on the Figure 2.7 contour plot. According to this mapping, lower node size ratios maximize the critical angle θ_m. At moderate node size ratios of 0.05-0.15, designs with the chirality angles between 50-70° could provide slightly higher values of θ_m than other designs.

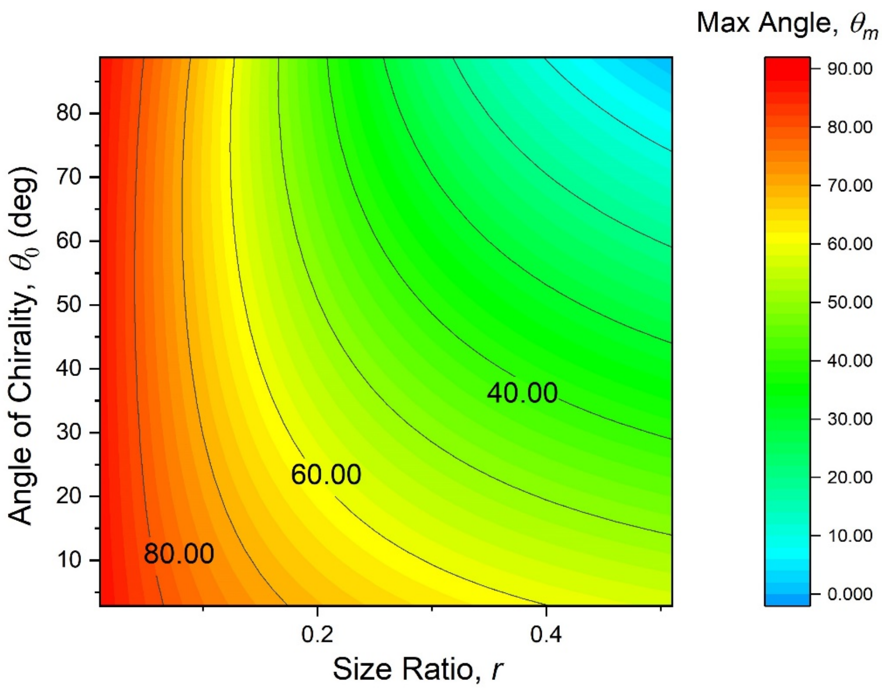

Fig.2.7: Contour map of the maximal allowed nodal rotation angle, θ_m. The corresponding maximal operational temperature of the metamaterial is $\Delta T_m = 2\theta_m(\mathrm{rad})/aL$.

3. Experimental Validation

For the metamaterials prototyping, a bimetal strip stock (SBC 721-112) by Shivalik Bimetal Controls Ltd. Index 721 stands for an alloy of 72% Mn, 10% Ni and 18% Cu, and 112 stands for the Invar alloy of 36% Ni and 64% Fe. Since the thermal bending coefficient in (2) is not a standard characteristic, we determined it experimentally. This value was found and used in Section 2 plots, when needed,

$$a = 0.24 \pm 0.01 \, \frac{\mathrm{rad}}{\mathrm{m{\cdot}^\circ C}} \tag{17}$$

Assembled samples had a nondeformed geometry with square nodes depicted in Figure 3.1, where the chirality angle, $\theta_0 = 45°$, and an equivalent nodal radius, $R = 4.56$ mm. Samples with three different values of the free standing bimetal strip length were fabricated, L_1 = 27.3 mm, L_2 = 54.9 mm, and L_3 = 81.4 mm. These correspond to the nodes size ratios, r_1 = 0.167, r_2 = 0.083, and r_3 = 0.056. Other parameters (a, θ_0, R) were identical in all samples. The samples were heated in a mini environmental chamber to a known uniform temperature ΔT, and their deformed geometry was captured through a clear window with a high resolution camera. A direct digital image processing procedure was applied to determine a change of nodal distance with temperature, interpreted in terms of the thermal strain, $\varepsilon_T = (l - l_0)/l_0$. Some of the captured deformed shapes are shown in Figure 3.2.

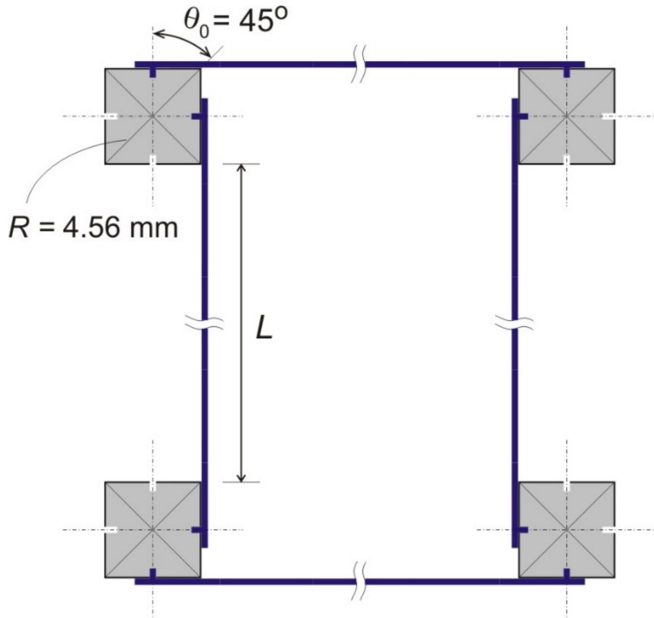

Fig. 3.1: Schematic diagram of a representative unit cell in fabricated samples. Square nodes imply a chirality angle, $\theta_0 = 45°$. Three different values of the length *L* were utilized.

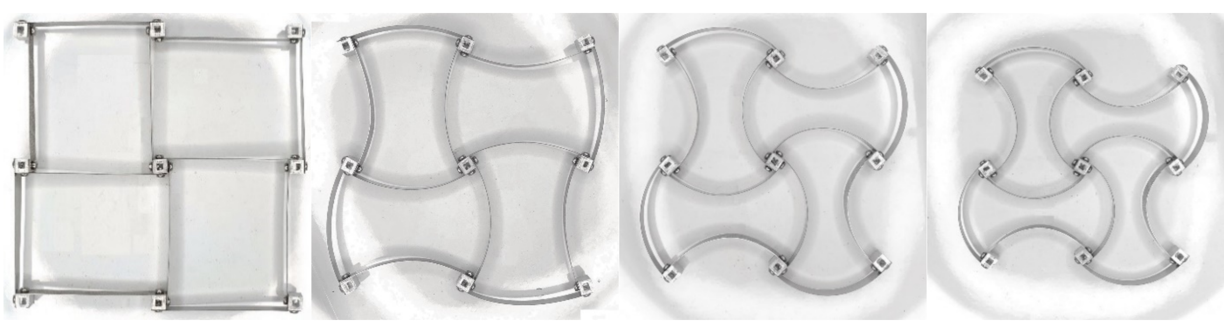

Fig.3.2: Recorded deformed shapes of a sample with *L* = 54.9 mm (refer to Figure 3.1), at four different temperatures ΔT (left-to-right): 0°C, 65°C, 85°C and 136°C.

The measured thermal strain values matched the theoretical curves well, as can be seen from Figure 3.3 plots. Given a 4% uncertainty in the *a*-value measurement, equation (17), plus an estimated $\pm$0.01 systematic thermal strain error due to geometrical imperfections of the samples, this match can be considered to be very good. This proves validity of the theoretical analysis approach discussed in Sections 2.1-2.5. The observed thermal strain dependence on temperature corresponds to a thermal expansivity, whose values can be best seen from the earlier, Figure 2.2 plot. For the temperature range of ΔT from $0℃$ to $130℃$, it is in the range of negative 0.0006-0.0041°C^{-1}. The initial thermal expansivity (at $\Delta T \approx 0℃$) is the range of negative 0.0006-0.0007°C^{-1}, depending on the value L.

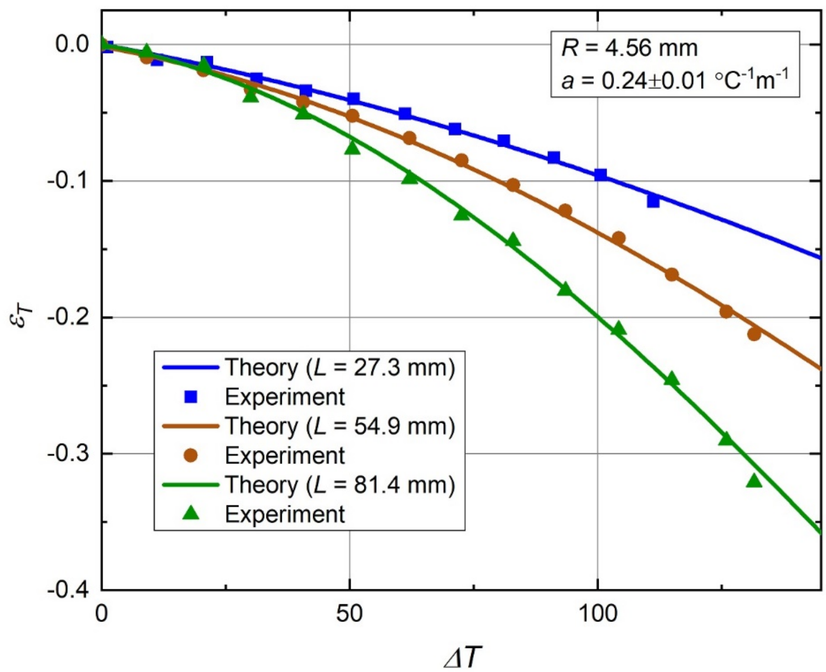

Fig.3.3: Behavior of the thermal strain (ε_T) with temperature; present theory and experiment.

4. Conclusions

Negative thermal expansion phenomenon is interesting and appealing for various scientific and engineering applications; however, it rarely occurs in natural materials. In this paper, we have discussed a universal antichiral thermomechanical metamaterial model with bimetal beams or strips connected at solid nodes. A theoretical analysis approach has been developed to write thermal expansivity of the metamaterial as an explicit function of temperature and only three design parameters: relative node size, chirality angle, and a bimetal constant. Experimental measurements follow the theoretical predictions well, where a thermal expansivity in the range of negative 0.0006-0.0041°C^{-1} has been seen.

In a future effort, the limit case configuration depicted in Figure 2.6 can be considered as an initial, room temperature architecture, where the bimetal strips are joint to each other at their middle points. This will probably lead to a lower negative thermal expansion effect, but will enhance mechanical properties of the metamaterial.

5. Acknowledgements

This work was supported by Gas Technology Institute, Des Plaines, IL, via the Sponsored Research Agreement #S858-22347. The authors are thankful to Dr. Alex Fridlyand and Dr. Miroslaw Liszka of Gas Technology Institute for their useful comments and discussions.

6. References

[1] Veselago, V.G. The electrodynamics of substances with simultaneously negative values of permittivity and permeability. *Soviet Physics Uspekhi* **1968**, *10*, 509-514.

[2] Smith, D.R.; Padilla,W.J.; Vier, D.C.; Nemat-Nasser, S.C.; Schultz, S. Composite medium with simultaneously negative permeability and permittivity. *Physical Review Letter* **2000**, *84*, 4184-4187.

[3] Pendry, J.B.; Holden, A.J.; Stewart, W.J.; Youngs, I. Extremely low frequency plasmons in metallic mesostructures. *Physical Review Letter* **1996**, 76, 4773-4776.

[4] Pendry, J.B.; Holden, A.J.; Robbins, D.J.; Stewart, W.J. Magnetism from conductors and enhanced nonlinear phenomena. *IEEE Trans. Microwave Theory Technology* **1999**, *47*, 2075-2084.

[5] Pendry, J.B. Negative refraction makes a perfect lens. *Physical Review Letter* **2000**, *85*, 3966-3969.

[6] Soukoulis, C.;Wegener, M. Past achievements and future challenges in the development of three-dimensional photonic metamaterials. *Nature Photonics* **2011**, *5*, 523-530.

[7] Zhou, J.; Koschny, T.; Kafesaki, M.; Economou, E.N.; Pendry, J.B.; Soukoulis, C.M. Saturation of magnetic response of split-ring resonators at optical frequencies. *Physical Review Letter* **2005**, *95*, 223902.

[8] Miyamaru, F.; Saito, Y.; Takeda, M.W.; Hou, B.; Liu, L.; Wen, W.; Sheng, P. Terahertz electric response of fractal metamaterial structures. *Physical Review Letter B* **2008**, *77*, 045124.

[9] Guariglia, E. Entropy and Fractal Antennas. *Entropy* **2016**, *18*, 84.

[10] Walser, R.M. Electromagnetic Metamaterials. *Proceedings SPIE 4467, Complex Mediums II: Beyond Linear Isotropic Dielectrics* **2001**.

[11] Cummer, S.A.; Christensen, J.; Alu, A. Controlling sound with acoustic metamaterials. *Nature Review Materials* **2016**, *1*, 16001.

[12] Hussein, M.I.; Leamy, M.J.; Ruzzene, M. Dynamics of phononic materials and structures: Historical origins, recent progress, and future outlook. *Applied Mechanics Rev*iews **2014**, *66*, 040802.

[13] Lui, Z.; Zhang, X.; Mao, Y.; Zhu, Y.; Yang, Z.; Chan, C.; Sheng, P. Locally resonant sonic materials. *Science* **2000**, *289*, 1734-1736.

[14] Wang, Y.Z.; Li, F.M.; Huang, W.-H.; Jiang, X.; Wang, Y.-S.; Kishimoto, K. Wave band gaps in two-dimensional piezoelectric/piezomagnetic phononic crystals. *International Journal of Solids and Structures* **2008**, *45*, 4203-4210.

[15] Yu, X.L.; Zhou, J.; Liang H.Y.; Jiang, Z.Y.; Wu, L.L. Mechanical metamaterials associated with stiffness, rigidity and compressibility: A brief review. *Progress in Materials Science* **2018**, *94*, 114-173.

[16] Bertoldi, K.; Vitelli, V.; Christensen, J.; van Hecke, M. Flexible Mechanical Metamaterials. *Nature Review Materials* **2017**, *2*, 17066.

[17] Kolpakov A.G. On the determination of the averaged moduli of elastic gridworks. *Prikl. Material Mekh*. **1985,** *59*, 969-977.

[18] Lakes, R.S. Foam structures with a negative Poisson's ratio. *Science* **1987**, *235*, 1038-1040.

[19] Lakes, R.S. Negative Poisson's ratio materials. *Science* **1987**, *238*, 551.

[20] Kaminakis, N.T.; Stavroulakis, G.E. Topology optimization for compliant mechanisms, using evolutionary- hybrid algorithms and application to the design of auxetic material. *Composites Part B: Engineering* **2012**, *43,* 2655-2668

[21] Stavroulakis, G.E. Auxetic behaviour: Appearance and engineering applications. *Physica Status Solidi B* **2005**, *242,* 710-720.

[22] Dong, L.; Lakes, R. Advanced damper with high stiffness and high hysteresis damping based on negative structural stiffness. *International Journal of Solids and Structures* **2013**, *50*, 2416–2423.

[23] Tan, X.; Chen, S.; Wang, B.; Zhu, S.; Wu, L.; Sun, Y. Design, fabrication, and characterization of multistable mechanical metamaterials for trapping energy. *Extreme Mech. Lett.* **2019**, *28*, 8-21.

[24] Dudek, K.K.; Gatt, R.; Grima, J.N. 3D composite metamaterial with magnetic inclusions exhibiting negative stiffness and auxetic behavior. *Materials and Design* **2020**, *187*, 108403.

[25] Nicolau, Z.G.; Motter, A.E. Mechanical metamaterials with negative compressibility transitions, *Nature Materials* **2012**, *11*, 608.

[26] Nicolau, Z.G.; Motter, A. E.; Longitudinal inverted compressibility in super-strained metamaterials. *Journal of Statistical Physics* **2013**, *151*, 1162.

[27] Chen, M.L.; Karpov E.G. Bistability and thermal coupling in elastic metamaterials with negative compressibility. *Physical Review E*. **2014**, *90*, 033201.

[28] Imre, A.R. Metamaterials with negative compressibility – a novel concept with a long history. *Materials Science-Poland* **2014**, *32*, 126–129.

[29] Karpov, E.G.; Danso, L.A.; Klein, J.T. Negative Extensibility Metamaterials: Occurrence and Design Space Topology. *Physical Review E* **2017**, *96*, 023002.

[30] Klein, J.T.; Karpov, E.G. Negative extensibility metamaterials: Phase diagram calculation. *Computational Mechanics* **2018**, *62*, 669-683.

[31] Karpov, E.G. Structural Metamaterials with Saint-Venant's Edge Effect Reversal. *Acta Materialia* **2017**, *123*, 245-254.

[32] Karpov, E.G.; Danso, L.A.; Klein, J.T. Anomalous strain energy transformation pathways in mechanical metamaterials. *Proceedings of the Royal Society A* **2019**, *475*, 20190041.

[33] Danso, L.A.; Karpov, E.G. Reprogramming Static Deformation Patterns in Mechanical Metamaterials. *Materials* **2018**, *11*, 2050.

[34] Karpov, E.G.; Danso, L.A. Strain Energy Spectral Density and Information Content of Materials Deformation. *International Journal of Mechanical Sciences* **2018**, *148*, 676-683.

[35] Coulais, C.; Sounas, D.; Alu, A. Static non-reciprocity in mechanical metamaterials. *Nature* **2017**, *542*, 461-464.

[36] Takenaka, K. Negative thermal expansion materials: technological key for control of thermal expansion. *Science and Technology of Advanced Materials* **2012**, *13*, 013001.

[37] Shen, X.; Viney, C.; Johnson, E.R.; Wang, C.; Lu, J.Q. Large negative thermal expansion of a polymer driven by a submolecular conformational change. *Nature Chemistry* **2013**, *5*, 1035-1041.

[38] Wu, L.; Li, B.; Zhou, J. Isotropic Negative Thermal Expansion Metamaterials. *ACS Applied Materials and Interfaces* **2016**, *8*, 17721-17727.

[39] Klein, J.T.; Karpov, E.G. Bistability in thermomechanical metamaterials structured as three-dimensional composite tetrahedra. *Extreme Mechanics Letters* **2019**, *29*,100459.

[40] Wu, W.; Hua, W.; Qian, G.; Liao, H.; Xud, X.; Berto, F. Mechanical design and multifunctional applications of chiral mechanical metamaterials: A review. *Materials and Design* **2019**, 180, 107950

[41] Gatt, R.; Grima, J.N. Negative compressibility, Phys. Status Solidi RRL **2008**, *2*, 236-238.

[42] Timoshenko, J. Analysis of Bi-Metal Thermostats. *Journal of the Optical Society of America* **1925**, *11*, 233-255.